Charge, mass, and energy changes during fragmentation of relativistic nuclei

W. R. Binns,[a] J. R. Cummings,[b] T. L. Garrard,[c] M. H. Israel,[a] J. Klarmann,[a]
E. C. Stone,[c] and C. J. Waddington[b]
[a]*Department of Physics and the McDonnell Center for the Space Sciences, Washington University, St. Louis, Missouri 63130*
[b]*School of Physics and Astronomy, University of Minnesota, Minneapolis, Minnesota 55455*
[c]*George W. Downs Laboratory, California Institute of Technology, Pasadena, California 91125*
(Received 31 October 1988)

We have examined the fragmentation of relativistic lanthanum and gold nuclei incident on targets of polyethylene, carbon, aluminum, and copper. Attention has been concentrated on those fragments whose atomic numbers were only changed by $+1$ to -3 from those of the incident nuclei. The cross section for the production of fragments with increased charge is about 10% that for fragments that have lost one charge, or about 1% of the total interaction cross section. We find that the velocity distributions of these fragments can be explained by assuming that they also lose significant numbers of neutrons when they pick up or lose charge, without a need to invoke any energy or momentum loss in the interaction, although we cannot exclude small losses. In particular, we cannot confirm the recent report of large energy losses during the charge pickup process. The relative numbers of neutrons lost can be represented by a simple Gaussian model, and, for those fragments with decreased charge, are much larger than the proton losses. These fragments consequently have large proton excesses and will be highly unstable.

INTRODUCTION

In reactions where nuclei are bombarded by energetic protons, (p-A) interactions, the largest partial cross sections measured are those for the production of secondary, or fragment, nuclei which have lost only a few nucleons, and hence have had only a small charge change, ΔZ. Extensive measurements of the yields for various isotopes from different targets have been reported by many workers. Recent compilations of individual references to these results have been given by Silberberg *et al.*[1,2] These measurements have also shown that there is a significant but appreciably smaller cross section for a "pickup" process, in which the charge of the final nucleus is increased over that of the target nucleus by one, or even two, charge units, rather than decreased. In general in this process the nuclei examined have had their masses reduced by neutron losses, e.g., Kaufman and Steinberg[3] observed $^{195}_{80}$Hg and $^{193}_{80}$Hg produced from a $^{197}_{79}$Au target. Similar effects are seen in nucleus-nucleus (A-A) interactions. For example Bachelier *et al.*[4] have observed 950 MeV/nucleon ^{20}Ne incident on a ^{27}Al target producing ^{20}Na by charge exchange with excitation of the delta resonance, see e.g., Norbury *et al.*[5] The same authors remark that they saw no nuclei with a mass number of >20 and that in fact no examples of pure proton pickup have ever been reported.

In (A-A) interactions, and in particular, in the work to be described here, it is the residual beam nucleus, rather than the residual target nucleus, that is the fragment under examination. In the earlier work[6-8] on these interactions, studies were restricted to lighter beams, with $A \leq 56$, but more recently[9-11] it has become possible to study the fragments of beams of energetic nuclei as heavy as ^{197}Au or ^{238}U. Of particular note for this study, which is concerned with the interactions of energetic gold and lanthanum nuclei in various targets, is the observation that the cross sections for the pickup process become relatively large as the charge of the nuclei increase and hence, easier to measure.

In earlier analyses, Silberberg and Tsao,[12] and Silberberg *et al.*[1] used data from (p-A) interactions to derive semiempirical relations to calculate the expected cross sections for those interactions with small charge changes. They found that at proton energies above a few hundred MeV the cross sections for small charge losses are hundreds of millibarns, mb, while for charge pickup, assumed to be due to (p,xn) interactions, they are tens of mb. These pickup cross sections are quite strongly energy and charge dependent, decreasing by a factor of 2 between 500 and 1000 MeV and increasing by a factor of $\approx$2.5 from ^{139}La to ^{197}Au, e.g., see Fig. 13. They also predict that the number of neutrons lost during the pickup is quite considerable, with a mean between four and five for La and six and seven for Au. In this work we have found qualitatively comparable results for (A-A) and (A-p) interactions, but the details show significant quantitative differences between the predictions and our measured values.

Using beams of relativistic La and Au nuclei incident on targets of polyethylene (CH_2), carbon, aluminum, and copper, we find pickup cross sections that are generally tens of mb at beam energies from 500 to 1250 MeV/nucleon. These fragments were detected by ionization and Cherenkov detectors, see Fig. 1. In these reactions the projectile $_{57}$La and $_{79}$Au nuclei emerge from the interactions as $_{58}$Ce and $_{80}$Hg, respectively. Similarly there is abundant production, with cross sections of hundreds of mb, of fragments with small charge losses. We are unable to resolve the individual masses of these pro-

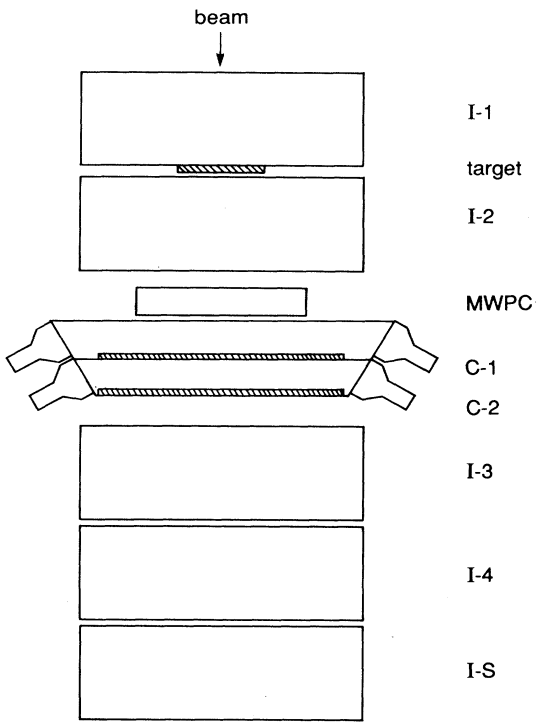

FIG. 1. Schematic diagram of the detector array. The thickness of each target used is given in Table I.

duced nuclei so we cannot study in detail the nature of the processes that produce these nuclei. However, the change in velocity, due to ionization energy losses experienced by a fragment between the point of creation in the target and its measurement in the Cherenkov detector, depends on its mass as well as its charge. Thus, by studying the velocity distribution of the fragments in the Cherenkov detector, we can draw conclusions about the distribution of their masses. Similarly, by looking at the small numbers of fragments produced in the front ion chambers during runs when there was no target present, where the effects of ionization losses are much less, the relative importance of any energy transfers in the interaction become more evident.

This analysis of the mass and energy changes is particularly interesting in light of the recent report by Gerbier *et al.*[11] of a large down shift in momentum of the fragment nucleus occurring in the interaction. That report is based on an examination of the charge pickup occurring when gold nuclei are incident on glass and aluminum targets. The apparent down shift in momentum is of the order of 3 to 4 GeV/c, which is difficult to explain as occurring in an interaction which has to be regarded as being extremely peripheral in nature, involving only a few of the nucleons in each nucleus. We will show that a more plausible, and entirely consistent explanation of our observations can be obtained by following the example of the semiempirical model and assuming a significant loss of neutrons during the small ΔZ changes (both positive and negative). This implies that for the $\Delta Z = +1$ fragments produced by these heavy beams the contribution from charge pickup due to the delta resonance is negligible, since in this process there is no mass change.

EXPERIMENTAL

These measurements were made with the Bevalac accelerator at the Lawrence Berkeley Laboratories, using as detectors an array of thin walled parallel plate ionization chambers and two 1.3 g/cm^2 thick plastic radiator Cherenkov counters, shown schematically in Fig. 1. These Cherenkov counters had threshold energies around 330 MeV/nucleon and gave signals that are strong functions of velocity in the energy regime just above the threshold. These signals, C_i, produced by a particle of velocity $\beta, = v/c$, can be very well described by a simple Cherenkov model of the form

$$C_i = C_0 Z^2 \left[1 - \frac{1}{(\beta n_{\text{eff}})^2} \right],$$

with a single effective index of refraction, n_{eff}, of 1.55 and a constant C_0. This model is valid for all values of $1.17 \leq 1/\beta^2 \leq 2.23$ $(0.67 \leq \beta \leq 0.93)$, as determined from our own calibration measurements of these detectors.[13] This array is used to identify the nuclei entering and emerging from moderately thin targets of various materials exposed to the incident beams of nuclei. The thicknesses of these targets were chosen to be ≤ 0.2 of an interaction mean free path and such that each beam should lose ≈ 100 MeV/nucleon while traversing them. These thicknesses are listed in Table I, together with the calculated energies of the beam nuclei at the center of the target (cot) and the energy losses, ΔE, incurred in each target. The detector system is similar to, but improved from that described by us recently,[9] both because of the use of two separate Cherenkov counters, which allow for unambiguous identification of most of those nuclei that interact in the detector, and because of the use of more and better ion chambers. Comparison of the ionization chamber signals with those from the Cherenkov counters determines the charge and velocity of each fragment that traverses the array, with a charge resolution which ranges from 0.1 to 0.2 of a charge unit. Examples of the data are shown in Fig. 2 for 1163 and 515 MeV/nucleon (cot) La nuclei incident on a polyethylene target, as well as for 543 MeV/nucleon (at the target position) La nuclei incident on the array during a "blank" run. In both cases where there was a target, a clearly defined population of nuclei with $\Delta Z = +1$ can be seen, in addition to the well separated groups of fragments with negative ΔZ. In the blank run a few fragments produced in the front ion chambers can still be seen.

The number of nuclei with $\Delta Z = +1$, together with the number of incident nuclei and the known conditions of the exposure, should allow us to calculate the partial cross sections for the production of these "pickup" nuclei, and compare them with the cross sections for the production of nuclei with negative ΔZ's. We have quoted values of these cross sections only in those cases for which we had acceptable blank runs at a corresponding energy. In addition, due to the trigger requirements im-

posed in the array, we have had to deduce the absolute numbers of incident nuclei from a knowledge of the total interaction cross sections, as determined by us previously.[9,14] The individual runs for which we could determine reliable cross sections are listed in Table I, together with the cross sections determined in this work for $\Delta Z=+1$ and -1 to -3. In principle we could also determine cross sections for those fragments with $\Delta Z=0$, since the beam peak does show a pronounced shoulder that has to be due to fragments that have only lost neutrons. However, the assumption of a Gaussian distribution for the mass losses that we make later does not allow us to calculate these cross sections with confidence. Hence, we note here only that there is evidence for cross sections of the order of half a barn for a neutron stripping interaction. The quoted errors in Table I are not merely statistical but also reflect our estimates of the systematic uncertainties. For this analysis we have generally restricted our attention to those beam energies which produced fragments whose velocities were low enough for the Cherenkov signal to be strongly dependent on the velocity of the fragment. The higher energy data will be reported elsewhere.

ANALYSIS

The scatter plots of the ionization and Cherenkov signals, C_i, given in Fig. 2, show clearly resolved bands for the fragments of each charge. The statistical fluctuations in the observed signals cause the events in these bands to be distributed about an ideal theoretical Cherenkov versus ionization track. For beams with energies only slightly greater than the Cherenkov threshold energy these bands show a wide spread in C_i. The distribution of C_i within each band can be readily determined for all cases except for $\Delta Z=\pm 1$, where overlap from the dominating beam distribution introduces confusion. For each

TABLE I. Beams, energies in the center of the targets (cot), in MeV/nucleon, target material and thicknesses, in g/cm^2, and energy loss in the target, in MeV/nucleon, and partial cross sections, in mb, for $\Delta Z=+1$ and -1 to -3.

Beam	E(cot) MeV/nucleon	Type	Target thickness (g/cm^2)	ΔE MeV/nucleon	Cross section $\Delta Z=+1$	Cross section $\Delta Z=-1$	Cross section $\Delta Z=-2$	Cross section $\Delta Z=-3$
La	515	CH_2	0.779	56	32.7±1.8	301.2±4.9	186.6±3.6	143.5±3.1
La	516	C	0.935	53	30.3±3.0	308.2±8.2	153.1±5.0	116.5±4.4
La	515	Al	1.096	55	39.6±5.2	356.3±12.5	160.8±6.6	113.5±5.7
La	515	Cu	1.250	55	62.1±10.4	552.6±25.1	185.1±11.5	148.2±10.7
La	616	CH_2	1.761	118	30.6±1.3	268.7±3.7	181.2±2.9	131.7±2.4
La	621	C	2.057	109	28.0±1.9	281.7±5.8	149.7±4.0	117.2±3.6
La	618	Al	2.400	113	28.7±2.3	336.3±7.0	163.0±4.3	125.1±3.8
La	618	Cu	2.724	112	44.1±3.7	386.9±9.6	173.9±4.7	130.8±4.1
La	773	CH_2	1.761	110	21.8±1.0	238.9±3.4	157.3±2.7	131.6±2.4
La	777	C	2.057	102	22.3±1.6	247.8±5.2	148.1±3.8	105.9±3.3
La	775	Al	2.400	106	39.6±5.2	356.3±12.5	160.8±6.6	113.5±5.7
La	775	Cu	2.724	105	25.8±3.0	320.6±9.0	172.4±4.9	130.7±4.3
La	1163	CH_2	1.761	100	19.9±1.2	203.0±3.8	125.6±2.8	103.0±2.5
La	1166	C	2.057	93	21.7±1.6	224.3±5.3	121.3±3.4	100.2±3.1
La	1165	Al	2.400	96	27.9±2.3	274.6±7.3	138.9±4.0	115.9±3.5
La	1165	Cu	2.724	96	42.6±4.1	305.2±12.5	151.8±5.6	125.8±4.9
Au	555	CH_2	1.252	118	81.2±2.1	430.5±5.0	214.9±2.9	163.1±2.4
Au	557	C	1.520	113	144.3±4.5	438.3±8.8	180.5±4.4	127.4±3.6
Au	557	Al	1.715	113	192.4±6.6	661.9±14.6	193.8±5.0	142.7±4.1
Au	559	Cu	1.929	111	333.7±12.0	855.0±26.3	213.3±6.8	150.5±4.9
Au	663	CH_2	1.252	110	43.4±1.7	338.6±4.6	196.6±3.0	159.0±2.6
Au	666	C	1.520	105	37.1±2.8	299.2±7.4	160.9±4.0	126.1±3.4
Au	666	Al	1.715	106	65.8±5.1	308.9±11.8	188.3±5.0	133.9±4.0
Au	667	Cu	1.929	104	63.2±9.0	268.5±22.6	209.6±6.6	140.7±5.0
Au	764	CH_2	1.252	106	35.0±1.5	292.4±4.3	198.1±3.2	147.5±2.7
Au	766	C	1.520	102	31.9±2.4	280.9±6.9	156.9±4.2	108.7±3.4
Au	766	Al	1.715	103	27.6±3.9	281.2±10.0	172.8±4.9	131.7±4.1
Au	767	Cu	1.929	101	18.7±7.2	262.1±18.3	181.0±6.3	141.1±5.1
Au	914	CH_2	1.252	101	30.5±1.4	275.7±4.2	176.0±3.1	141.3±2.7
Au	915	C	1.520	97	30.9±2.0	297.0±6.2	152.0±3.8	111.9±3.3
Au	915	Al	1.715	98	40.1±3.0	322.1±8.9	171.4±4.5	116.6±3.7
Au	915	Cu	1.929	97	49.8±5.9	402.4±19.0	207.0±7.4	142.7±5.5

of these two bands there is a significant overlap with the beam distribution and we have determined the C_i distributions by considering only those events that are in the half of the band that contains signals that deviate from the theoretical track in the direction away from the region of overlap with the beam distribution.

The natural resolution of the detector is given by the width of the peak produced by the beam particles during a blank run, as shown as an example in Fig. 3(a) for a particular beam at a particular energy. For runs with a target the C_i distributions for the beam particles show a wide tail to lower values, see e.g. Fig. 3(b), due to the presence of fragments which have experienced a mass loss but no charge loss. Similarly the fragments with nonzero ΔZ have C_i distributions that are wider than expected from the natural resolution. These wide distributions and the wide tail are due to the strong dependence of these signals on the velocity of the particles, and suggest that the fragments have a distribution of velocities. The mean values of the Cherenkov signals, $\langle C_i \rangle$, for fragments of each charge, should be expected, to first order, to show a simple Z^2 dependence, provided the fragments have the same velocity as the beam. However, the distributions of C_i/Z^2 for the 616 MeV/nucleon (cot) La beam on the polyethylene target, illustrated in Fig. 3(b), show instead that on average the $\Delta Z = +1$ fragments

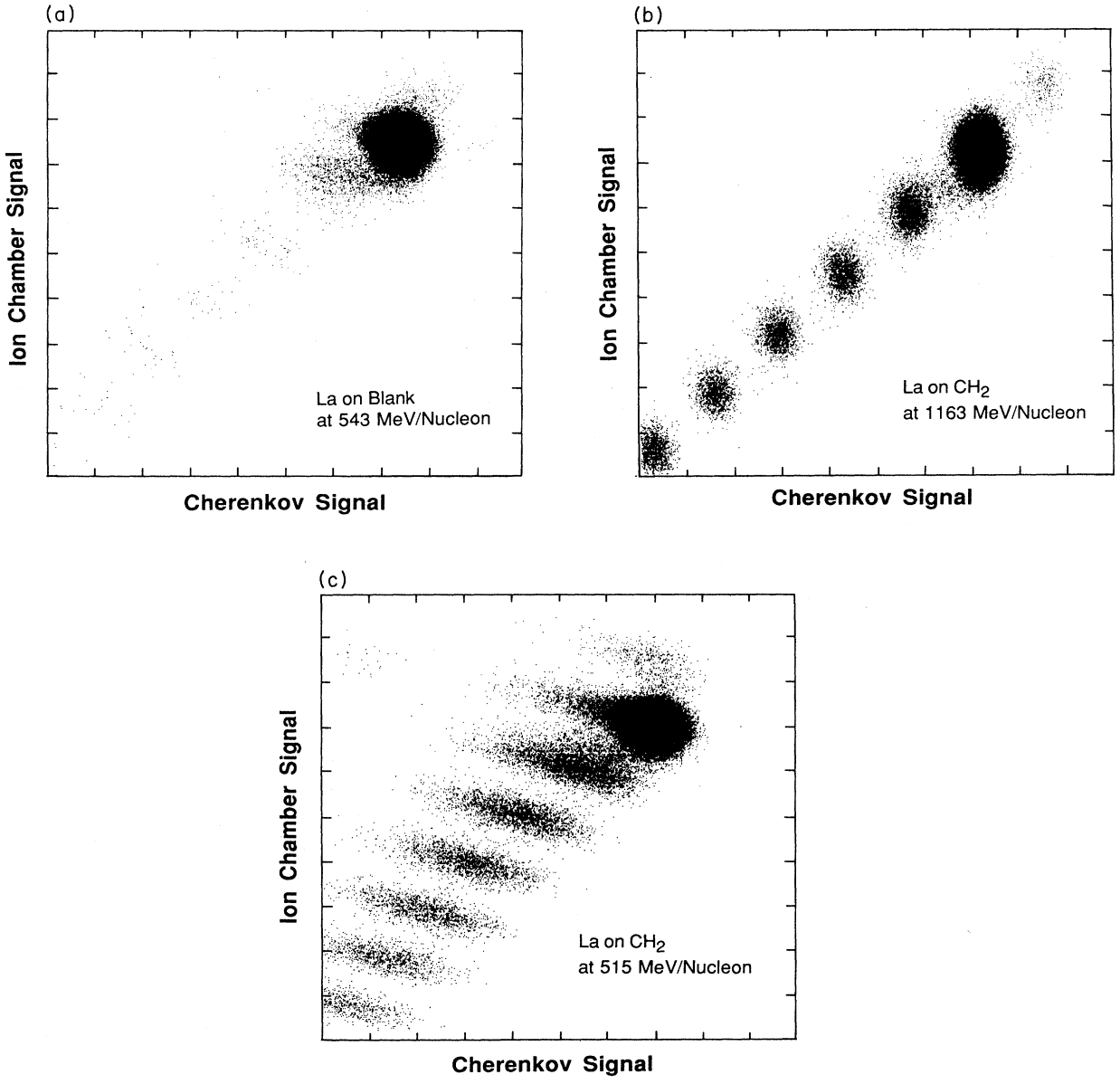

FIG. 2. Ionization signals versus Cherenkov signals for La nuclei of 543 MeV/nucleon at the target position with no target, and for La nuclei of 1163 and 515 MeV/nucleon in the target incident on a polyethylene target.

have experienced a significant shift of the mean velocity relative to that of the beam nuclei. Similar shifts are seen for the fragments with charge losses.

In what follows we show that both the shift and spread in the signals are best explained by the assumption that the fragments with small charge changes experience relatively large median mass changes. The alternative assumption, that the fragments suffer a large, and ΔZ dependent, energy loss in the interaction, with only a minimal mass change, does not appear to be well supported by the evidence. If the mass changes invoked are large enough, and have a wide enough range, it becomes unnecessary to assume that any significant velocity change occurs in the interaction itself.

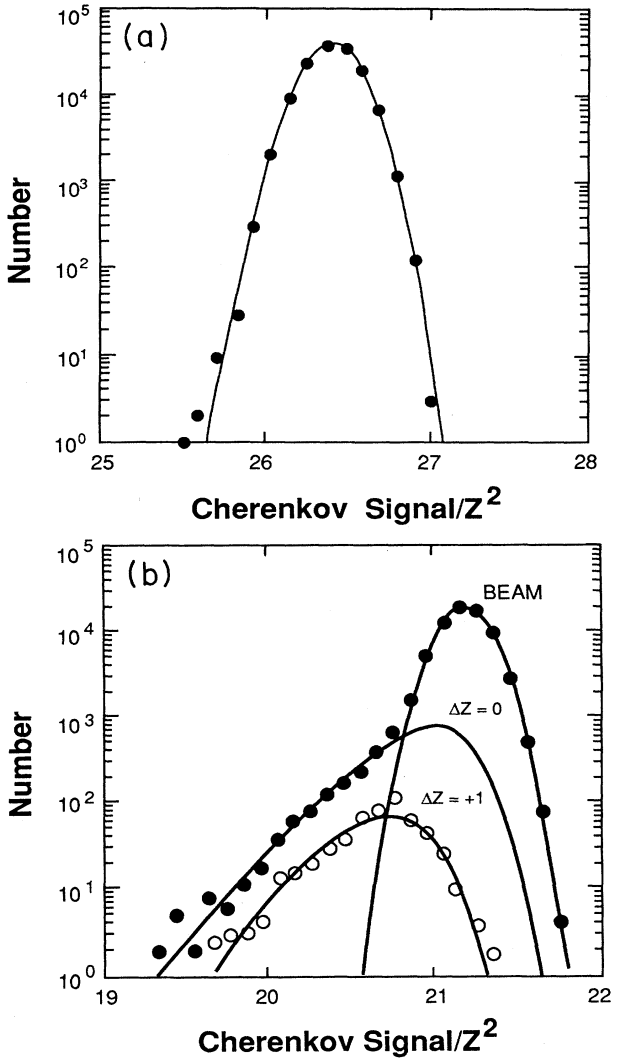

FIG. 3. (a) Observed distribution of Cherenkov signals for a blank run of 675 MeV/nucleon La nuclei when no target was present. Data points are shown fitted by a Gaussian distribution. (b) Fitted distributions of Cherenkov signals, normalized by Z^2, for beam particles, and particles with $\Delta Z = +1$, for the La beam incident at 700 MeV/nucleon on a polyethylene target and having 616 MeV/nucleon at the center of the target (cot) and 499 MeV/nucleon at the center of the radiators. These fits were derived using the procedures described later. The data points, ●, for the beam particles have been fitted with a Gaussian distribution for the noninteracting beam particles and a lower signal tail consisting of particles that interacted with no charge change, but a mass change. The data points, ○, for the $\Delta Z = +1$ particles are fitted with a curve whose derivation is described later.

The Cherenkov detector gives a signal that is dependent on Z and β, but the β of each fragment is reduced from the value it has at the interaction by the energy losses that occur in the target and the matter of the detector below the target, which is predominantly that in the Cherenkov radiators themselves. In any one event the nucleus first loses energy as a beam particle until it reaches the point of the interaction, and then loses more energy as a fragment while it emerges from the target and traverses the detector material. These energy losses, expressed as an energy per nucleon, depend on Z, A, and β, since the same energy loss may be shared between a different number of nucleons. Since the energy changes due to these losses are quite small, the energy loss rate, (dE/dx), in the matter of the target and the detector can be considered to be the same for each particle, apart from the Z^2 dependence.

Let E_b be the incident beam energy, in MeV/nucleon, and E_f be the energy of the fragment at the center of the Cherenkov detector, also in MeV/nucleon. Also let x_1 be the target thickness before the point of interaction and x_2 the thickness from the point of interaction to the center of the Cherenkov detector, so that $x_{\text{tot}} = x_1 + x_2$. Then the energy loss per nucleon ΔE_b of the noninteracting beam nuclei of mass A_b in the target plus the detector is given in terms of the proton energy loss per unit thickness, (dE/dx), by

$$\Delta E_b = \frac{Z_b^2}{A_b}\left\{\frac{dE}{dx}\right\}(x_{\text{tot}}) .$$

If the energy change per nucleon in the interaction is ΔE_i, then the energy, E_f, of a fragment with mass and charge of A_f and Z_f is

$$\begin{aligned} E_f &= E_b - \left\{\frac{x_1}{x_{\text{tot}}}\right\}\Delta E_b \\ &\quad - \left\{\frac{x_2}{x_{\text{tot}}}\right\}\left\{\frac{A_b}{A_f}\right\}\left\{\frac{Z_f}{Z_b}\right\}^2 \Delta E_b - \Delta E_i , \\ &= E_b - \left\{\frac{dE}{dx}\right\}\left[\frac{Z_b^2}{A_b}x_1 + \frac{Z_f^2}{A_f}x_2\right] - \Delta E_i . \end{aligned}$$

For a particular fragment species, and assuming a thin target, there would be an equal number of nuclei for every dx, leading to a rectangular distribution on a C_i plot. Since these targets have finite thickness the distributions are slightly modified by an exponential falloff in abundance. Figure 4(a) shows such distributions for various values of A_f, for $\Delta Z = +1$, charge pickup, for the case of the 616 MeV/nucleon (cot) La beam on a polyethylene target. Here we assume that $\Delta E_i = 0$, and we

have looked at a range of values of A_f corresponding to neutron losses of up to 12 neutrons. These distributions are normalized to have a constant area.

If these theoretical distributions are convolved with a Gaussian experimental spread in the signals derived from the peak of the noninteracting beam nuclei, then the resulting distributions are like those given in Fig. 4(b). Similar distributions for $\Delta Z=-1$ are shown in Fig. 5. No one of the distributions for the $\Delta Z=+1$ case can fit the experimental data, which are shown on Fig. 6(a), together with the combination of distributions needed to provide a fit. An examination of similar data for the $\Delta Z=-1$ fragments, Fig. 6(b), shows that they also can be fitted only by a combination of distributions which include those having values of A_f that imply that a considerable number of neutrons may be lost along with one proton.

The distributions for C_i/Z^2 for the isotopes overlap and cannot be resolved individually. However, if we adopt the hypothesis that the mean mass loss, $\langle \Delta A \rangle$, should have a Gaussian distribution, then we obtain fits to the data, with good values of reduced χ^2. Hence, we have determined the mean mass loss, and the spread in that mean mass loss, $\sigma_{\Delta A}$, by fitting to a relation for the cross section for each isotope, $\phi(\Delta A,\Delta Z)$, in terms of the total cross section, $\Phi(\Delta Z)$, of the form

$$\phi(\Delta A,\Delta Z)$$
$$=\frac{\Phi(\Delta Z)}{\sigma_{\Delta A}(2\pi)^{1/2}}\exp\left[-0.5\left[\frac{(\langle \Delta A\rangle-\Delta A)}{\sigma_{\Delta A}}\right]^2\right],$$
$$\text{for } \Delta A \geq \Delta A_{\min}$$
$$=0, \quad \text{for } \Delta A < \Delta A_{\min}$$

suitably normalized by multiplying by a factor Ψ, given by

$$\Psi=\frac{\Phi(\Delta Z)}{\sum_{\Delta A=\Delta A_{\min}}^{\Delta A_{\max}}\phi(\Delta A,\Delta Z)},$$

and

$$\Delta A_{\min}=\text{abs.}[\Delta Z]\cdots \text{for negative } \Delta Z\ ;$$
$$\Delta A_{\min}=0\cdots \text{for } \Delta Z=+1,0\ .$$

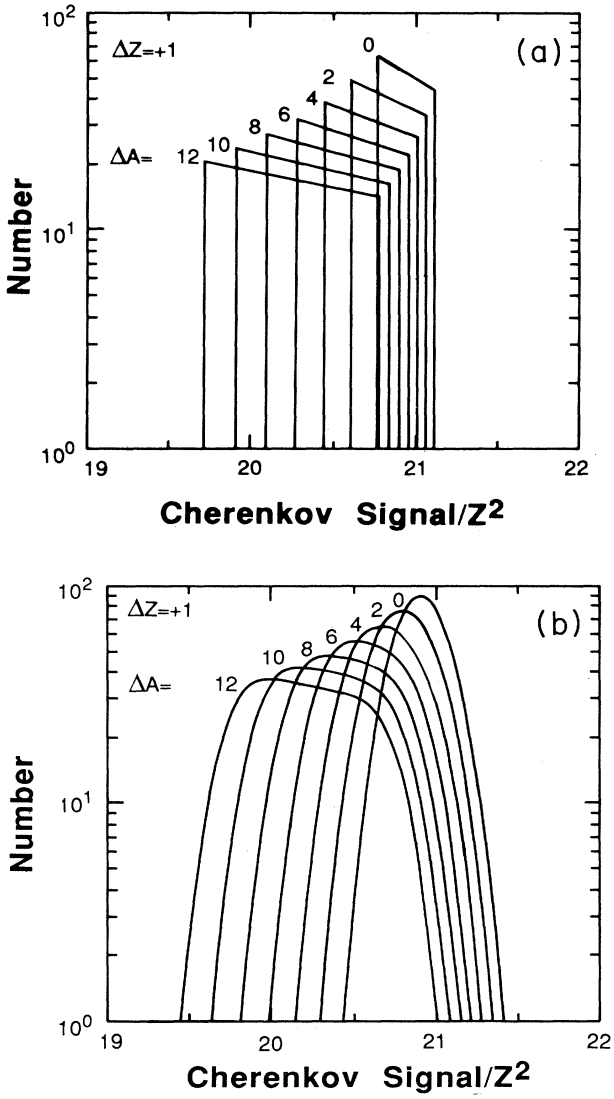

FIG. 4. (a) The idealized distributions of the Cherenkov signals, normalized by Z^2, for fragments with $\Delta Z=+1$, with $\Delta A=0,2,4,6$, etc., produced by the 616 MeV/nucleon (cot) La beam on a polyethylene target. These distributions are normalized to a common area. (b) The idealized distributions convolved with the response function derived from the beam distribution of the normalized Cherenkov signals for fragments with $\Delta Z=+1$, with $\Delta A=0,2,4,6$, etc., produced by the 616 MeV/nucleon (cot) La beam on a polyethylene target. These distributions are normalized to a common area.

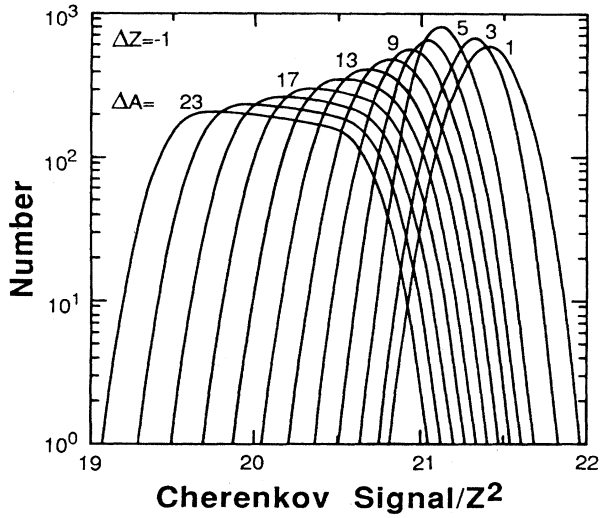

FIG. 5. The same as Fig. 4(b) but for $\Delta Z=-1$, and with $\Delta A=1,3,5$, etc.

These Gaussian distributions are thus truncated at the low mass loss end so that the cross sections are zero for a mass loss less than the charge loss. The median mass losses, ΔA, are thus not equal to $\langle \Delta A \rangle$ but can be determined from the fit. Figures 6(a) and (b) show the fits to the data obtained for two examples of $\Delta Z = +1$ and -1, in the case of 616 MeV/nucleon (cot) La nuclei on a polyethylene target. These fits then give the best values for $\langle \Delta A \rangle$ and $\sigma_{\Delta A}$. These mean values, and the reduced χ^2 values for each fit, are given in Table II for four different targets and two beams at various energies for fragments with $\Delta Z = +1$, -1, -2, and -3. We did make a similar analysis for those fragments with $\Delta Z = 0$. However, the assumption of a Gaussian distribution of mass losses was apparently inadequate to let us calculate reliable values for the fitting parameters, never giving reduced χ^2 values that are acceptable. Also shown in Table II are the determined values for the median mass losses, assuming $\Delta E_i = 0$, and the median mass losses predicted from the semiempirical relations for a hydrogen target.

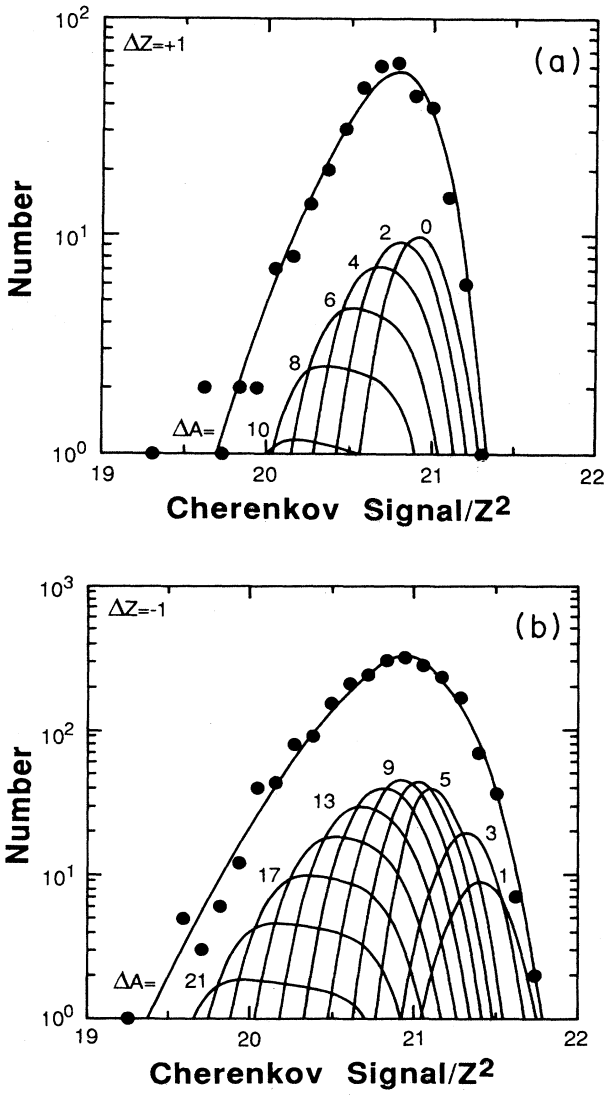

FIG. 6. (a) The Gaussian distributions of the response functions fitted to the experimental data for fragments with $\Delta Z = +1$, with $\Delta A = 0,2,4$, etc., produced by the 616 MeV/nucleon La beam on a polyethylene target. These distributions have areas that would sum to the total area under the data points. (b) The same for $\Delta Z = -1$, but with $\Delta A = 1,3,5$, etc.

We can explain our data by invoking neutron losses and assuming that no energy is lost in the interaction, i.e., $\Delta E_i = 0$. However, this is in contrast with the result reported[11] for Au nuclei at 730 MeV/nucleon of an energy loss of ≥ 14.3 MeV/nucleon.[15] We can estimate a reasonable upper limit to ΔE_i, by assuming there is no mass change for the $\Delta Z = +1$ fragments, which would correspond to a charge exchange. These upper limits are given in Table III, as ΔE for $\Delta n = 0$, and can be seen, in every case, to be much less than that reported by Gerbier *et al.*,[11] and less than the nucleon binding energy of the nuclei.

In Figs. 7(a) and (b) we show that the calculated energy losses for $\Delta Z = +1$ fragments as a function of the beam energy for La and Au nuclei incident on all four targets. These energy losses are calculated under three different assumptions as follows.

(1) That there was no mass loss, just charge exchange.

(2) That the neutron loss was that predicted by the semiempirical relations[1,12] for a hydrogen target.

(3) That the neutron loss was the median value determined from our own fitting procedure.

It can be seen that assumptions (2) and (3) give values in fair agreement and are consistent with a minimal energy loss. Assumption (1) gives upper limits to the energy losses of some 3–5 MeV/nucleon. As mentioned before, it has been reported by Gerbier *et al.*[11] that for gold nuclei with a mean energy of 730 MeV/nucleon interacting in a glass target and with a mean energy of 880 MeV/nucleon interacting in an aluminum target, the $\Delta Z = +1$ fragments show evidence that these authors interpret as implying an energy loss in the interactions. From their data we can recalculate these mean losses to be 14.3 ± 1.7 MeV/nucleon in the glass and 18.2 ± 2.2 MeV/nucleon in the aluminum.[15] These values greatly exceed the binding energy of the nucleons in the nucleus. For the physical setup described in Ref. 11, assuming our best value of about four nucleons for the mass loss of Au nuclei with these energies, Table II, would lead to a mean energy loss due to ionization of 1.9 and 7.0 MeV/nucleon relative to the beam for interactions in the glass and aluminum, respectively.[16] The dependence of the calculated energy losses on target mass, A_{targ}, is quite weak in every case. Hence, the use of glass and aluminum targets by Gerbier *et al.*[11] cannot be the reason for the difference between their reported result and that derived from our analysis at very similar energies.

Examining the data from the target runs does not allow us to distinguish cleanly between energy loss and mass loss in the interactions. However, we also made runs with no target present, and in these the few fragments produced in the gas and thin foils of the ion chambers allow us to deduce another estimate of these

TABLE II. Fitting parameters and median mass losses, as determined, and as calculated from the semiempirical relation (Refs. 1 and 12) (S and T). Also shown are the reduced chi squares for the fits. Errors shown on the fit parameters include both statistical and systematic uncertainties.

Lanthanum beam				Number of nucleons lost			
E	Target	Number interacted	Peak of Gaussian	σ of Gaussian	ΔA median from fit	S and T median	Reduced chi sqr
				$\Delta Z=+1$			
515	CH_2	347	6.25±0.31	3.42±0.35	6.35±0.23	3.83	1.03
516	C	150	7.65±0.51	3.66±0.66	7.71±0.42		1.40
515	Al	129	6.63±0.77	4.43±0.83	6.92±0.48		1.32
515	Cu	79	5.94±1.59	5.44±1.64	6.73±0.75		0.93
616	CH_2	363	1.99±0.73	4.65±0.32	3.76±0.28	3.85	0.49
621	C	148	4.21±0.94	3.76±0.69	4.71±0.54		1.18
618	Al	155	5.09±0.77	3.75±0.70	5.41±0.48		0.67
618	Cu	244	4.79±0.72	4.29±0.56	5.38±0.39		1.05
773	CH_2	283	−4.71±2.53	4.75±0.49	1.55±0.40	3.85	0.88
777	C	147	0.73±1.92	4.63±0.69	3.13±0.61		0.69
775	Al	169	3.52±1.25	3.93±0.74	4.28±0.64		0.83
775	Cu	164	3.06±1.32	3.29±0.69	3.64±0.76		1.04
				$\Delta Z=-1$			
515	CH_2	1629	9.20±0.31	7.28±0.23	10.24±0.16	6.99	1.48
516	C	734	4.09±1.01	10.69±0.45	9.12±0.31		1.76
515	Al	531	6.86±0.88	9.36±0.50	9.75±0.35		0.78
515	Cu	263	8.73±0.96	7.98±0.64	10.22±0.46		0.86
616	CH_2	2276	10.38±0.14	4.79±0.13	10.50±0.11	7.09	1.56
621	C	1022	10.14±0.24	5.20±0.22	10.34±0.18		0.80
618	Al	1133	9.43±0.26	5.48±0.22	9.79±0.17		2.14
618	Cu	1376	9.84±0.25	5.92±0.21	10.26±0.17		0.70
773	CH_2	2205	11.70±0.15	3.54±0.17	11.70±0.15	7.14	2.52
777	C	1090	11.75±0.22	3.56±0.27	11.75±0.21		1.26
775	Al	1045	11.91±0.24	4.17±0.29	11.93±0.23		1.12
775	Cu	1288	13.03±0.22	3.47±0.30	13.03±0.21		1.35
				$\Delta Z=-2$			
515	CH_2	2257	15.60±0.15	5.88±0.13	15.65±0.14	11.87	0.96
516	C	837	14.30±0.35	7.31±0.32	14.65±0.25		0.87
515	Al	578	15.27±0.39	6.95±0.35	15.46±0.31		1.53
515	Cu	271	13.72±0.84	8.53±0.74	14.47±0.49		1.09
616	CH_2	3104	14.10±0.10	4.55±0.09	14.12±0.10	11.99	2.46
621	C	1134	13.67±0.22	5.63±0.20	13.78±0.19		1.46
618	Al	1213	3.66±0.22	5.66±0.20	13.77±0.18		0.87
618	Cu	1367	13.79±0.20	5.44±0.17	13.87±0.17		2.53
773	CH_2	2730	14.65±0.14	4.60±0.15	14.66±0.14	12.04	1.98
777	C	1183	14.26±0.26	5.49±0.27	14.33±0.23		1.39
775	Al	1072	14.61±0.25	4.96±0.28	14.64±0.24		0.51
775	Cu	1213	14.80±0.28	5.65±0.29	14.87±0.25		1.12
				$\Delta Z=-3$			
515	CH_2	1721	20.14±0.16	5.58±0.14	20.14±0.15	15.78	1.52
516	C	618	20.25±0.34	7.04±0.32	20.28±0.32		0.96
515	Al	398	19.49±0.43	6.92±0.39	19.54±0.40		1.07
515	Cu	197	20.10±0.58	6.29±0.56	20.12±0.56		1.09
616	CH_2	2311	18.66±0.12	4.65±0.10	18.66±0.12	15.87	1.11
621	C	880	18.46±0.22	5.13±0.20	18.47±0.22		1.60
618	Al	915	18.28±0.22	5.30±0.20	18.28±0.22		1.17
618	Cu	1000	18.50±0.22	5.55±0.20	18.51±0.22		1.96
773	CH_2	2313	19.52±0.15	4.55±0.15	19.52±0.15	15.95	1.52
777	C	849	18.89±0.29	5.39±0.29	18.90±0.28		1.12
775	Al	841	19.80±0.27	4.76±0.29	19.80±0.27		1.58
775	Cu	906	20.01±0.29	5.24±0.31	20.01±0.29		0.72

TABLE II. (*Continued*).

	Gold beam		Number of nucleons lost				
E	Target	Number interacted	Peak of Gaussian	σ of Gaussian	ΔA median from fit	S and T median	Reduced chi sqr
			$\Delta Z = +1$				
555	CH_2	516	6.79±0.46	4.68±1.02	7.14±1.12	5.62	1.38
557	C	246	4.91±1.35	6.50±1.32	6.57±0.63		0.87
557	Al	331	3.65±0.86	5.08±0.69	4.98±0.37		1.10
559	Cu	493	3.40±0.72	5.12±0.55	4.85±0.30		2.61
663	CH_2	482	2.97±0.97	7.04±0.45	5.79±0.36	5.60	1.27
666	C	215	5.74±0.99	5.36±0.73	6.56±0.54		1.20
666	Al	299	5.73±0.90	6.04±0.64	6.88±0.44		1.02
667	Cu	192	1.88±1.88	7.26±0.84	5.39±0.60		1.42
764	CH_2	363	0.34±1.37	5.01±0.47	3.21±0.40	5.63	0.91
766	C	173	1.71±1.77	4.46±0.72	3.48±0.65		1.11
766	Al	202	2.86±1.46	4.67±0.71	4.26±0.63		1.40
767	Cu	251	0.25±1.82	5.75±0.64	3.68±0.55		0.85
			$\Delta Z = -1$				
555	CH_2	3284	12.82±0.55	14.44±1.05	15.34±0.26	8.10	1.93
557	C	1449	6.70±1.15	14.76±0.89	12.62±0.37		1.24
557	Al	1778	4.29±1.13	15.13±0.69	11.83±0.32		2.58
559	Cu	2421	3.80±1.13	16.82±0.71	12.44±0.28		4.75
663	CH_2	2946	12.78±0.19	6.84±0.16	13.09±0.14	8.30	2.95
666	C	1499	10.82±0.43	8.71±0.31	12.09±0.23		1.22
666	Al	1592	10.94±0.43	8.89±0.30	12.25±0.22		1.91
667	Cu	1050	10.09±0.60	9.44±0.38	11.89±0.30		1.98
764	CH_2	2427	14.90±0.18	5.33±0.20	14.92±0.17	8.43	0.84
766	C	1213	14.30±0.29	5.80±0.33	14.36±0.25		0.89
766	Al	1368	14.44±0.32	6.99±0.33	14.63±0.25		0.87
767	Cu	1485	14.85±0.30	6.79±0.32	14.99±0.25		1.69
			$\Delta Z = -2$				
555	CH_2	3958	21.51±0.29	9.35±0.24	21.46±0.26	13.02	1.65
557	C	1349	20.84±0.56	10.19±0.58	20.86±0.46		1.40
557	Al	1385	19.85±0.53	10.52±0.61	20.06±0.39		1.07
559	Cu	1594	20.05±0.54	11.25±0.67	20.26±0.38		1.67
663	CH_2	3588	18.23±0.15	6.70±0.13	18.28±0.14	13.20	2.72
666	C	1472	17.31±0.27	7.33±0.25	17.44±0.23		1.36
666	Al	1470	17.38±0.28	7.63±0.26	17.55±0.23		1.61
667	Cu	860	17.42±0.43	8.52±0.40	17.71±0.33		2.10
764	CH_2	2981	18.64±0.16	5.73±0.16	18.65±0.16	13.38	2.15
766	C	1176	17.72±0.31	6.61±0.33	17.77±0.28		1.54
766	Al	1212	16.92±0.32	7.03±0.33	17.04±0.27		1.02
767	Cu	1177	17.84±0.32	6.77±0.32	17.91±0.29		2.67
			$\Delta Z = -3$				
555	CH_2	2851	26.04±0.26	7.67±0.17	26.04±0.26	17.57	0.83
557	C	867	25.39±0.50	7.97±0.39	25.40±0.49		0.98
557	Al	883	25.72±0.55	8.93±0.42	25.74±0.52		1.34
559	Cu	871	25.50±0.52	8.69±0.39	25.52±0.50		1.01
663	CH_2	2736	23.94±0.14	5.47±0.13	23.94±0.14	17.70	1.86
666	C	1055	22.99±0.26	6.17±0.24	22.99±0.26		1.65
666	Al	953	23.68±0.27	6.09±0.25	23.69±0.26		1.84
667	Cu	495	23.79±0.38	6.16±0.38	23.79±0.38		1.08
764	CH_2	2167	24.92±0.18	5.12±0.18	24.92±0.18	17.80	1.25
766	C	768	24.67±0.33	5.30±0.37	24.67±0.33		1.10
766	Al	842	24.13±0.33	6.39±0.34	24.13±0.33		0.80
767	Cu	796	25.19±0.35	6.37±0.36	25.19±0.35		1.14

losses. Since in the blank runs the amount of energy loss due to ionization is significantly less than that when a target was present, the observed C_i distribution depends differently on the assumed mass loss. In Figs. 8(a) and (b) we have compared the assumed losses needed to

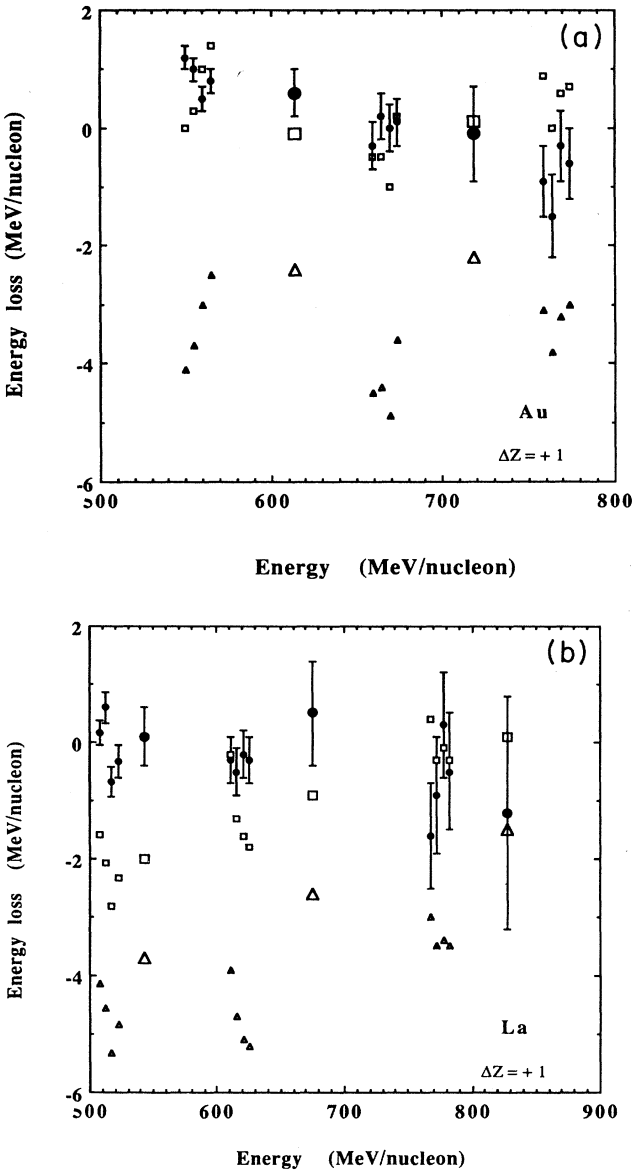

FIG. 7. (a) Calculated energy loss in the interaction, in MeV/nucleon, during charge pickup of Au nuclei as a function of beam energy, for three different assumptions on neutron loss. Points shown as ● with error bars assume the median neutron loss calculated from our fits to the data. Points shown as △ and □ correspond to assumptions 1 and 2, respectively (see text). Error bars of similar size have been omitted to reduce confusion. Similarly, for clarity of presentation the results for the four targets at any one beam energy have been symmetrically shifted in energy about the nominal true energy in the target so that they appear in increasing order of mass from left to right, (CH_2, C, Al, Cu). Values obtained from the blank runs based on the three assumptions are shown as oversize points. (b) As Fig. 7(a), but for La nuclei.

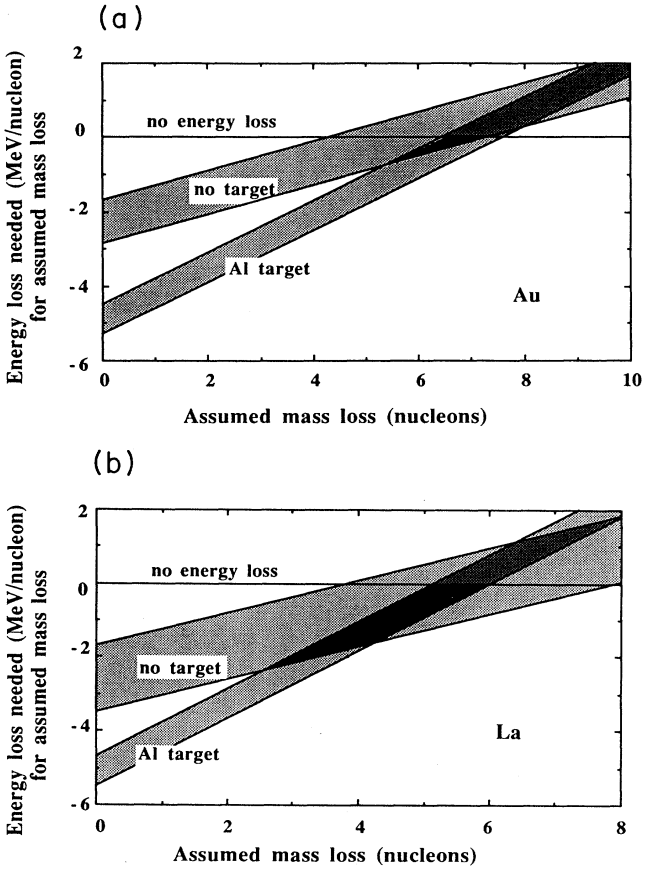

FIG. 8. (a) Calculated variation of energy loss with assumed median mass loss. Bands of width ±1 sigma for an Al target run and for a blank run are shown for Au beams of 600–700 MeV/nucleon. (b) Calculated variation of energy loss with assumed median mass loss. Bands of width ±1 sigma for an Al target run and for a blank run are shown for La beams of 600–700 MeV/nucleon.

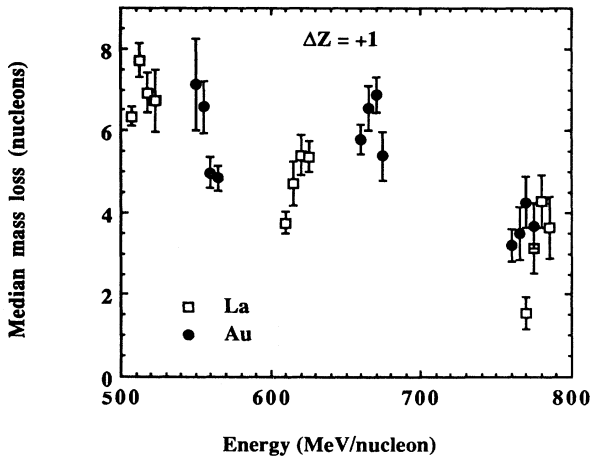

FIG. 9. Median mass loss as a function of beam energy for $\Delta Z = +1$ fragments for Au, solid symbols, and La, open symbols, beam nuclei, incident on four different targets. As in Fig. 7 these different targets are displayed by using small energy displacements and appear in increasing order of mass from left to right (CH_2, C, Al, Cu).

TABLE III. Calculated energy loss for $\Delta Z = +1$ fragments under three assumptions regarding the mass loss. All energies are in MeV/nucleon. The statistical errors in these calculated value are the same in each case.

Beam	E (cot)	Target	ΔE $\Delta n=0$	ΔE S and T	ΔE ΔA=fit	Error in ΔE
La	543	none	−3.75	−2.04	0.13	0.47
La	515	CH_2	−4.13	−1.59	0.17	0.21
La	516	C	−4.56	−2.08	0.59	0.26
La	515	Al	−5.31	−2.81	−0.68	0.25
La	515	Cu	−4.83	−2.32	−0.33	0.28
La	675	none	−2.55	−0.90	0.52	0.94
La	616	CH_2	−3.86	−0.22	−0.30	0.37
La	621	C	−4.72	−1.27	−0.47	0.43
La	618	Al	−5.10	−1.62	−0.16	0.41
La	618	Cu	−5.19	−1.76	−0.34	0.40
La	828	none	−1.54	0.06	−1.17	2.00
La	773	CH_2	−2.99	0.44	−1.63	0.90
La	777	C	−3.50	−0.27	−0.89	0.97
La	775	Al	−3.37	−0.12	0.25	0.95
La	775	Cu	−3.55	−0.31	−0.49	0.97
Au	614	none	−4.30	−2.02	−0.29	0.43
Au	555	CH_2	−4.12	0.04	1.20	0.16
Au	557	C	−3.67	0.33	1.03	0.22
Au	557	Al	−3.03	0.96	0.50	0.18
Au	559	Cu	−2.55	1.39	0.84	0.17
Au	614	none	−2.42	−0.14	0.60	0.44
Au	663	CH_2	−4.50	−0.46	−0.32	0.36
Au	666	C	−4.43	−0.52	0.18	0.40
Au	666	Al	−4.86	−0.96	−0.04	0.37
Au	667	Cu	−3.59	0.22	0.07	0.40
Au	718	none	−2.15	0.08	−0.07	0.78
Au	764	CH_2	−3.09	0.88	−0.86	0.61
Au	766	C	−3.81	0.02	−1.47	0.67
Au	766	Al	−3.20	0.61	−0.34	0.65
Au	767	Cu	−3.04	0.72	−0.61	0.64

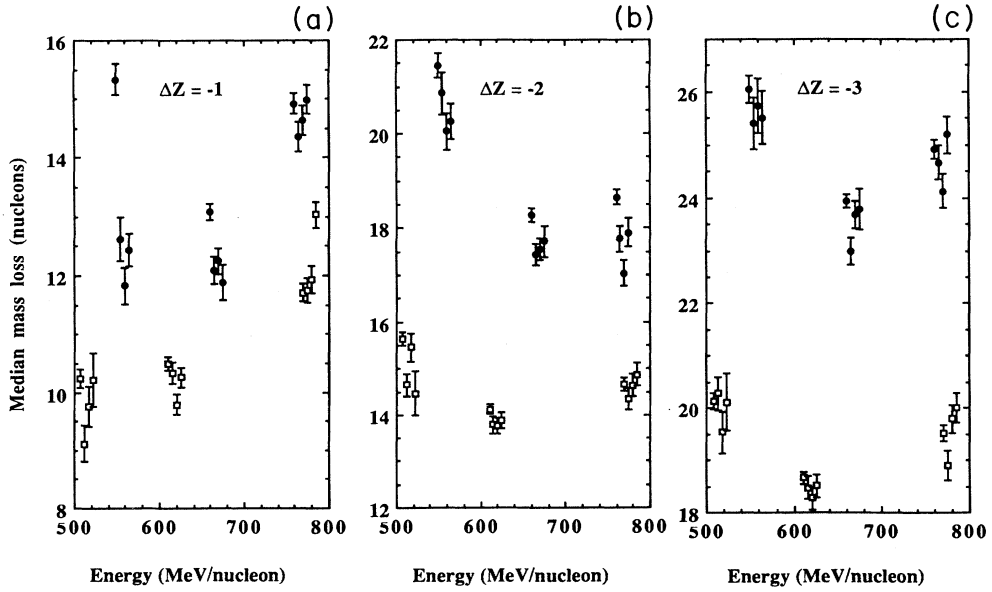

FIG. 10. (a), (b), and (c) Similar to Fig. 9 but for $\Delta Z = -1$, -2, and -3 fragments, respectively.

represent the data by plotting the calculated values of ΔE as a function of ΔA. These figures show bands that represent an uncertainty of plus and minus one standard deviation for La and Au beams of 600–700 MeV/nucleon, for the case of no target and of an aluminum target (Al targets are used in this comparison because most of the residual mass for the blank runs is composed of Al foils between the ionization chambers). Although the statistical weight of the blank runs is quite small, these bands overlap for only a rather small area in ΔE-ΔA space. If we neglect positive values of ΔE as unphysical then for both La and Au it appears that only rather small values of negative ΔE are allowed. This supports our conclusion that there are no significant energy losses in these interactions.

The mass losses that we deduce are relatively independent of the target. Figure 9 shows the median mass losses for $\Delta Z = +1$ fragments as a function of beam energy for the four targets for both the La and Au beams. It can be seen that overall there is little dependence on A_{beam} or A_{targ}, although there is some energy dependence, with ΔA decreasing as E increases. The one apparent exception, illustrated in Fig. 9 and listed in Table II, is afforded by the La on CH_2 targets, which give consistently lower values of ΔA, showing that there would be a marked difference for a pure hydrogen target. However, a similar effect is not seen for the Au beam. This could be a reflection of the presence of a closed neutron shell in $^{139}_{57}La_{82}$. Figs. 10(a), (b), and (c) show similar plots of the median mass loss as a function of the energy for the $\Delta Z = -1$, -2, and -3 fragments. Here also the results are generally independent of A_{targ}, again with the apparent exception of CH_2, but show a much stronger dependence on A_{beam}. In addition, for $\Delta Z = -1$ fragments ΔA tends to increase with increasing E, whereas for all the other fragments ΔA tends to decrease with increasing E.

The cross sections for the production of $\Delta Z = +1$ fragments in the various targets are shown in Fig. 11. We see

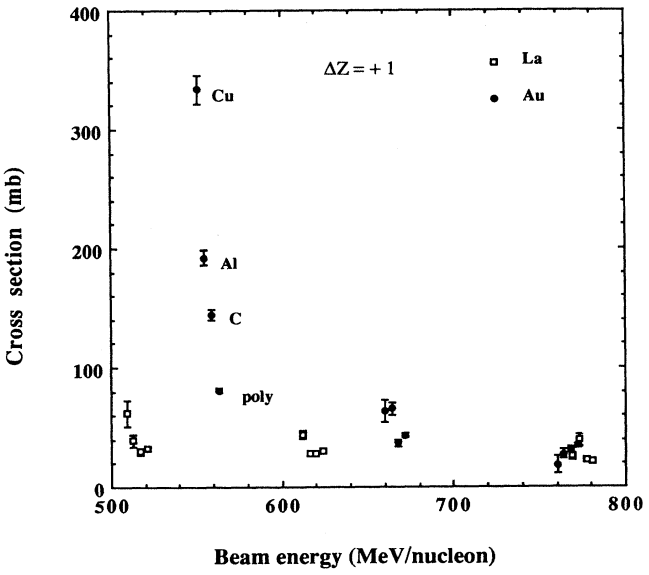

FIG. 11. Cross sections in mb as a function of beam energy for the production of $\Delta Z = +1$ fragments, for Au, solid symbols, and La, open symbols, beam nuclei, incident on four different targets. Unlike Figs. 7, 9, and 10, these different targets are displayed by using small energy displacements but appear in *decreasing* order of mass from left to right (Cu, Al, C, CH_2).

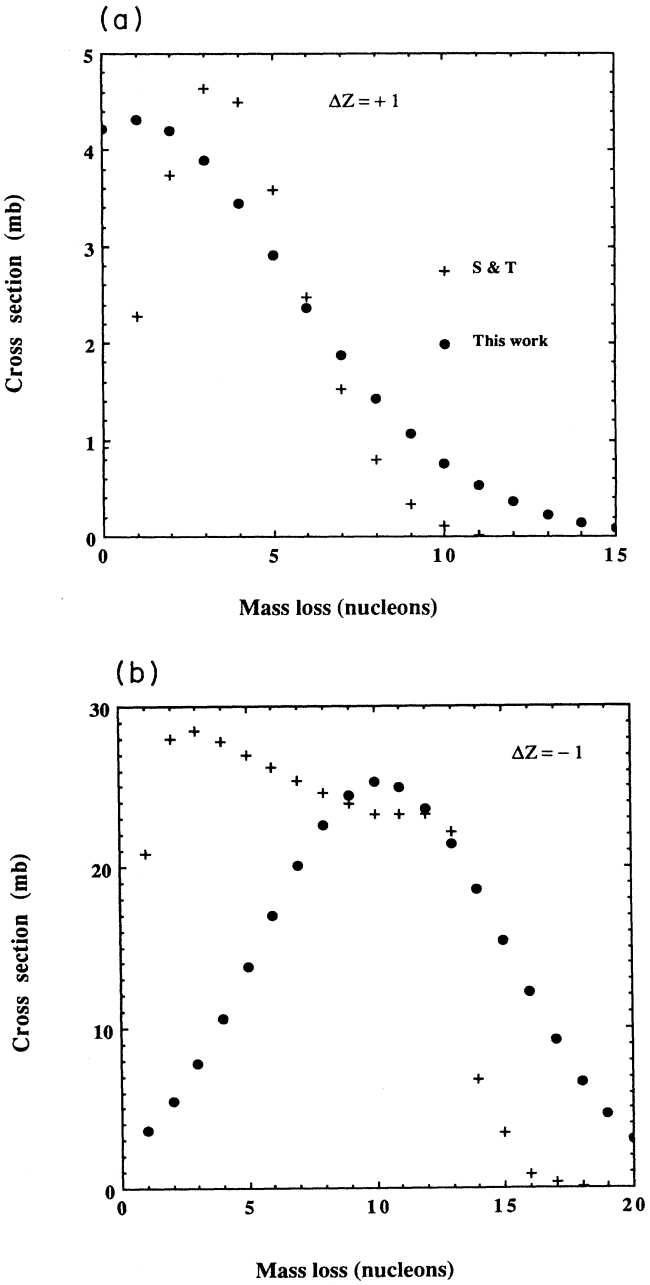

FIG. 12. (a) and (b) The cross sections in mb, as a function of the mass loss, for the case of La on a hydrogen target at 618 MeV/nucleon, as derived, solid symbols, and as predicted (Refs. 1 and 12), crosses, for $\Delta Z = +1$ and -1 fragments.

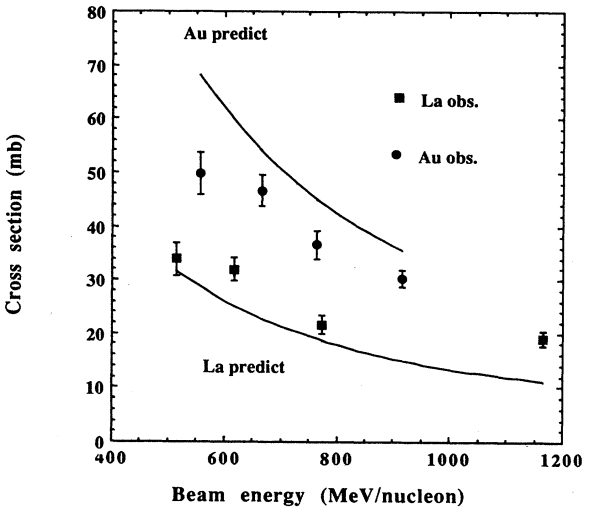

FIG. 13. Cross sections in mb as a function of beam energy for the production of $\Delta Z=+1$ fragments as derived from our measurements in a hydrogen target, solid symbols, and as predicted (Refs. 1 and 12), continuous curve. Circles for Au beam, squares for La beam.

a strong dependence on both A_{beam} and A_{targ} at the lowest energy, which rapidly disappears as the energy increases. The very large cross section for low energy Au on Cu, compared with that for Au on Al or La on Cu suggests that an additional pickup process that is strongly A_{targ} dependent becomes dominant as the energy decreases. This could represent the onset of a significant contribution from charge exchange processes; a conclusion that is consistent with the reduced values of $\overline{\Delta A}$ seen for the heavier targets in the lowest energy Au run, Table II.

We can compare the cross sections for hydrogen that we derive from a comparison of the carbon and polyethylene results[9] with those calculated from the semiempirical relations.[1,12] Table IV shows that the differences between these derived and predicted cross sections never exceed about 50%, which is in agreement with the claims made for the semiempirical relation that it should be accurate to within a factor of 2. The differences between our assumed distributions of mass losses and those predicted are quite small for the $\Delta Z=+1$ fragments, but become considerable for the $\Delta Z=-1$ fragments, as can be seen in Figs. 12(a) and (b). These cross sections show a general decrease with increasing energy, for both beams and all ΔZ, e.g., see Fig. 13, which shows the cross sections for the charge pickup case as a function of beam energy. It is also clear that there is a strong dependence on the mass of the beam. The calculated values of the median mass loss for all the small ΔZ fragments are given in Table II and can be compared with our values for carbon and polyethylene. It can be seen that the discrepancies become larger as ΔZ becomes more negative.

CONCLUSIONS

Our results do not confirm the large energy loss reported by Gerbier *et al.*[11] during the pickup process. Nor can we explain their results in terms of our assumed neutron losses. Such losses should not appreciably affect the energies of the products of their interactions which occur in the glass, since these energies are only slightly influenced by energy losses between the interaction and the point of observation. It might be appropriate to note that they observed only twelve pickup events in the glass, but their reported cross section, of 44±13 mb, is in reasonable agreement with our value for 915 MeV/nucleon (cot) Au on carbon of 30.3±1.6 mb.

Since these large energy losses appear to be physically implausible, and we have identified large neutron losses as a reasonable alternative explanation for our observations, we need to consider the consequences of these large

TABLE IV. Comparison between predicted and deduced cross sections for a hydrogen target.

Beam	E	ΔZ	Cross section mb	S and T	Beam	E	ΔZ	Cross section mb	S and T
La	515	1	33.9±3.1	31.6	Au	556	1	49.7±3.9	68.1
La	618	1	31.9±2.2	24.9	Au	665	1	46.6±2.9	54.1
La	774	1	21.6±1.7	18.6	Au	765	1	36.6±2.6	45.0
La	1165	1	19.0±1.3	11.1	Au	915	1	30.3±1.6	35.6
La	515	−1	297.7±8.4	339.4	Au	556	−1	426.6±8.7	367.2
La	618	−1	262.2±6.3	335.9	Au	665	−1	358.3±7.8	319.6
La	774	−1	234.5±5.7	333.7	Au	765	−1	298.2±7.3	279.8
La	1165	−1	192.4±4.2	326.9	Au	915	−1	265.1±4.8	226.6
La	515	−2	203.4±6.0	226.7	Au	556	−2	232.1±4.9	341.2
La	618	−2	197.0±4.8	246.8	Au	665	−2	214.5±4.9	349.8
La	774	−2	161.9±4.5	267.5	Au	765	−2	218.7±5.2	349.8
La	1165	−2	127.8±3.0	270.3	Au	915	−2	188.0±3.3	334.2
La	515	−3	157.0±5.1	84.7	Au	556	−3	181.0±4.0	160.1
La	618	−3	139.0±4.0	91.8	Au	665	−3	175.5±4.3	174.1
La	774	−3	144.5±4.0	95.3	Au	765	−3	166.9±4.4	180.2
La	1165	−3	104.4±2.7	86.3	Au	915	−3	156.0±2.9	176.7

neutron losses. Table II lists the median values of the mass loss found in each case. It can be seen that these estimates are essentially independent of the target, but rapidly increase with increasing proton loss. This suggests that the fragments produced, at least for small ΔZ, are generally very proton rich and will β decay to lower charge if given time. The stable end products of these fragmentations will thus result in an elemental distribution quite different from that observed in this type of experiment, where the nuclei are seen within a few nanoseconds of their production. The implications of this conclusion to the problem of cosmic ray propagation through the diffuse interstellar matter are considerable and shows that achieving isotopic resolution in these cross section measurements will be required before propagation can be correctly modeled.

Our conclusion that large numbers of neutrons are lost in these interactions is based on a velocity rather than a direct mass measurement. Hence, the exact details on the relative yields and any residual energy losses should be verified experimentally; either by adding fast neutron counters to a detector such as ours so that the neutron counts can be associated with individual events, or by making direct isotopic measurements of the masses of the fragments as they emerge from the target. Neither of these alternatives is technically feasible as yet, but the power of a Cherenkov detector working near its threshold to act as a velocity discriminator, that has been demonstrated in this experiment, could be further exploited in future runs.

ACKNOWLEDGMENTS

An experiment such as this can only be carried to a successful conclusion with the help of a large number of people. We are indebted to W. E. Althouse, J. A. Becker, J. W. Epstein, B. W. Gauld, and P. S. Gibner of our own groups. The personnel at Lawrence Berkeley Laboratory made the runs possible and we particularly wish to thank H. J. Crawford and J. M. Engelage for their help. This work was funded in part by NASA under Grant Nos. NAG-8-498, 8-500, and 8-502, and NGR 05-002-160, 24-005-050, and 26-008-001.

[1]R. Silberberg, C. H. Tsao, and J. R. Letaw, Astrophys. J. Suppl. **58**, 873 (1985).

[2]R. Silberberg, C. H. Tsao, and J. R. Letaw, *Proceedings of the 20th International Cosmic Ray Conference, Moscow, 1987,* edited by V. L. Kozyarivsky *et al.* (Nauka, Moscow, 1987), Vol. 2, p. 133.

[3]S. B. Kaufman and E. P. Steinberg, Phys. Rev. C **22**, 167 (1980).

[4]D. Bachelier *et al.*, Phys. Lett. B **172**, 23 (1986).

[5]J. W. Norbury, P. A. Deutchman, and L. W. Townsend, Nucl. Phys. **A433**, 691 (1985).

[6]G. D. Westfall, L. W. Wilson, P. J. Lindstrom, H. J. Crawford, D. E. Greiner, and H. H. Heckman, Phys. Rev. C **19**, 1309 (1979).

[7]D. L. Olson, B. L. Berman, D. E. Greiner, H. H. Heckman, P. J. Lindstrom, and H. J. Crawford, Phys. Rev. C **28**, 1602 (1983).

[8]W. R. Webber, J. C. Kish, and D. A. Schrier, *Proceedings of the 20th International Cosmic Ray Conference, Moscow, 1987,* edited by V. L. Kozyarivsky *et al.* (Nauka, Moscow, 1987), Vol. 2, p. 133.

[9]W. R. Binns, T. L. Garrard, M. H. Israel, M. P. Kertzman, J. Klarmann, E. C. Stone, and C. J. Waddington, Phys. Rev. C **36**, 1870 (1987).

[10]C. J. Waddington, Proceedings of the 8th High Energy Heavy Ion Study, 1988, Report LBL-24580, p. 430.

[11]G. Gerbier, Ren Guoxiao, and P. B. Price, Phys. Rev. Lett. **60**, 2258 (1988).

[12]R. Silberberg and C. H. Tsao, Astrophys. J. Suppl. **35**, 129 (1977).

[13]B. J. Newport, Ph.D. thesis, Caltech, 1986.

[14]M. P. Kertzman, Ph.D. thesis, University of Minnesota, 1988.

[15]After allowing for the energy loss of the Au nuclei in the matter above the glass detector the values for the momentum and velocity shift implied by taking the consistent values at the center of the glass of $E=730$ MeV/nucleon, $\beta=0.8281$, and $\Delta Z=+0.32$, are $\Delta p=-3.4$ GeV/c and $\Delta\beta=0.0033$, respectively, leading to $\Delta E=-4.3$ MeV/nucleon. For the aluminum target, the values are as follows: Energy at center of glass detector is still equal to 730 MeV/nucleon; $\Delta Z=+0.41$; $\Delta p=-4.36$ GeV/c; $\Delta\beta=0.004\,24$; $\Delta E=-18.2$ MeV/nucleon.

[16]It is not stated in Ref. 11 whether or not the ionization energy loss difference between different charge and mass fragments and the beam is taken into account. The difference in energy loss between the fragments and the beam particles, for a gold nucleus interacting in the center of the target, losing four nucleons and increasing charge by one, is -1.9 MeV/nucleon for the glass target and -7.0 MeV/nucleon for the aluminum target. For fragments with a small negative charge change, the energy losses are closer to those of the beam because of the opposing effects of charge decrease and mass decrease.